Electrochemical and surface studies of the effect of naphthalene-based additives on tin electrodeposition

Aranzales Ochoa, D.M.

CHAPTER 4

The effect of naphthalene-based additives on the kinetics of tin electrodeposition on a boron doped diamond electrode

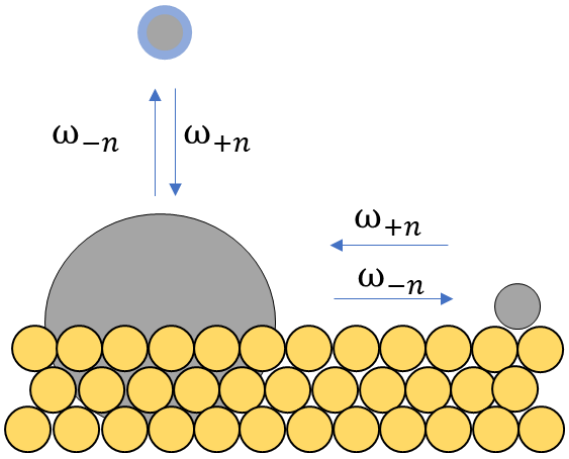

This chapter is based on the article: Aranzales, D.; Wijenberg, J. H. O. J.; Koper, M. T. M. The effect of naphthalene-based additives on the kinetics of tin electrodeposition on a boron doped diamond electrode. *Submitted to ChemElectroChem*.

Abstract

The effect of naphthalene-based additives: naphthalene (NPT), naphthalenesulfonate (NPTS) and hydroxynaphthalenesulfonate (HNPTS) on the kinetics of tin electrodeposition on a boron doped diamond (BDD) electrode has been studied by means of chronoamperometry and scanning electron microscopy (SEM). Potentiostatic current transients in the absence and the presence of naphthalene-based additives are analyzed by using the Scharifker-Hills model. A strong decrease of the kinetics of tin nucleation on BDD was observed in the presence of naphthalene-based additives, NPT showing the smallest effect and HNPTS showing the largest effect. From the long-term Cottrell behavior of the transients, similar values of tin (II) diffusion coefficients were obtained for all additives, suggesting that there is no complexation of Sn (II) by the additives and that the charge-transfer kinetics itself is not influenced by the presence of the additives. In the absence of additives, tin deposition on BDD displays a progressive nucleation and growth mechanism at less negative potential, switching to instantaneous nucleation and growth at more negative potential. In the presence of NPTS and HNPTS, progressive nucleation and growth transients are observed. The growth mode results are confirmed by the tin features observed in the scanning electron micrographs. In conclusion, NPT, NPTS and HNPTS mainly decrease the rate of the nucleation of tin deposition. In comparison, ethoxylated α-napthalenesulfonic acid (ENSA, a commonly used additive in the tin plating industry) inhibits tin deposition process on BDD even more strongly. These observations show a striking similarity to our previous study of tin deposition on gold electrodes.

4.1 Introduction

Tin electrodeposition is a low-cost and versatile process, widely used in corrosion protection and in the packaging industry. During the last years, new applications for tin plating in electronics and manufacturing have been developed[1] and since then, new challenges in the micro- and nanotechnology of the process have emerged. The production of high-quality tin coatings requires the addition of organic compounds in the electroplating baths, in order to obtain the desired chemical and physical properties of the metal deposits. Determining the role of these additives allows the optimization and enhancement of the tin deposition, and the extension of its applications.

Earlier studies of tin electrodeposition[2–4] have mainly focused on the use of metal[3,4] and glassy carbon substrates[5]. Following our previous work on tin electrodeposition on a gold substrate[6], we study here the effect of naphthalene-based derivatives, naphthalene (NPT), naphthalenesulfonate (NPTS) and hydroxynaphthalenesulfonate (HNPTS), on the kinetics of the nucleation and growth of tin electrodeposition on a boron doped diamond surface (BDD). This substrate has been considered as highly suitable to study metal deposition [7], [8], [9], [10] due to its high stability, reproducibility, and flat surface with height variation of ~5 nm over 5x5 µm areas. The relatively low defect density is expected to lead to a low nucleation rate. This facilitates nucleation and growth measurements by electrochemical transient experiments and in-situ microscopic techniques[7] .

4.2 Experimental details

Before each measurement all glassware was stored overnight in a solution of 1g L^{-1} $KMnO_4$ in 0.5 M H_2SO_4. Before use, it was rinsed with water and 30% hydrogen peroxide solution in order to remove permanganate anions and trace impurities. Glassware was boiled in water five times before starting the experiments. The water used to clean glassware and to prepare solutions was demineralized and ultra-filtrated by a Millipore MilliQ system (18.2 MΩ cm). A gold wire was chosen as a counter electrode and a reversible hydrogen electrode (RHE) was used as a reference, but all the potentials are referred to the normal hydrogen electrode (NHE).

Chronoamperometric experiments were performed using a potentiostat VSP-300 (Bio-logic). The electrode potential was corrected for Ohmic drop during the measurements, by using 85% of the Ohmic resistance measured by electrochemical impedance spectroscopy.

The working electrode was a boron doped diamond disk (BDD) (1 cm diameter, 1 mm thick). It was prepared before each experiment by mechanical and electrochemical methods. Firstly, it was polished during 5 minutes with diamond powder (0.05 μm particle size), and subsequently it was transferred to an ultrasound bath, and treated during 10 min in acetone and another 10 min in water. After mechanical polishing, the BDD electrode was electropolished by cycling 10 times between -0.74 to 1.56 V vs. NHE in 0.1 M H_2SO_4 solution at 50 mV s^{-1}. A cyclic voltammogram of the BDD surface was recorded in 0.1 M H_2SO_4 solution at potentials between -0.74 to 1.56 V at 50 mV s^{-1} before starting the measurements in order to check the cleanliness of the electrode surface.

The morphology of tin deposit was observed ex situ by scanning electron microscopy SEM. Micrographs were taken using the model JEOL 820 SEM at 2 - 10 kV. Low voltages were chosen due to the semiconductor nature of BDD electrode.

All solutions were prepared from chemicals with the highest purity commercially available: H_2SO_4 (96% ultrapure, Merck), $SnSO_4$ (≥ 95%, Sigma Aldrich), naphthalene (≥ 99%, Sigma Aldrich), 2-napthalenesulfonic acid sodium salt (99.6%, Sigma Aldrich), sodium thiosulfate (≥ 99.99%, Sigma Aldrich), 4-hydroxy-1-naphthalenesulfonic acid sodium salt (≥ 95 %, Santa Cruz Biotechnology) and ethoxylated α-napthalenesulfonic acid (73.6%, Pulcra chemicals). In the case of ENSA the main impurities are sulfuric acid with 8.7 %, and water with 2.4 %, other impurities were not provided by the supplier.

4.3 Results and discussion

4.3.1 Chronoamperometric transients

Figure 1 shows the cyclic voltammogram for tin electrodeposition and electro-dissolution on a BDD electrode (under static conditions, i.e., no rotation). The voltammogram exhibits a broad cathodic wave with a peak at -0.266 V, and a sharp anodic peak at -0.156 V, characteristic of Sn (II) reduction and Sn (0) oxidation, respectively. The cyclic voltammogram was used as a reference to choose the potential region to record the current transients, as indicated by the red lines, from -0.220 to -0.460 V.

Figure 2 presents the recorded current transients for tin electrodeposition without additives; transients show rising currents related with the nucleation and growth processes, followed by a current decay caused by the overlap of the growing nuclei and at longer times by mass transport limitations. The recorded current transients exhibit shorter peak times and higher current maxima with increasingly negative potential[7]. This behavior is usual for nucleation and growth processes, provided the substrate is not being strongly modified over the range of applied potentials[11].

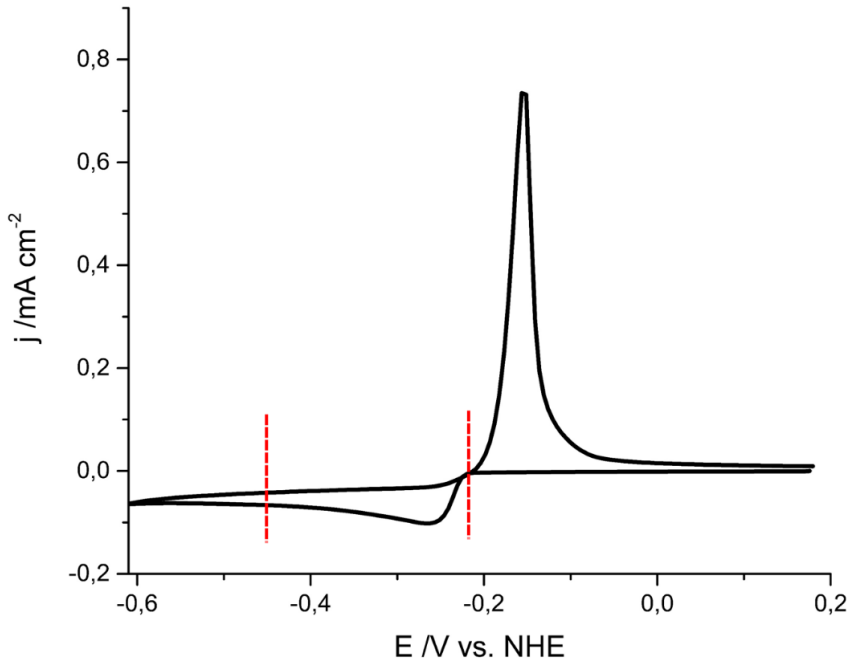

Figure 1. Cyclic voltammogram of tin electrodeposition on a boron doped diamond surface in 0.1 M H_2SO_4 and 0.5 mM $SnSO_4$. CV recorded between -0.61 to 0.19 V at 30 mV s^{-1}. Red-dashed lines indicate the potential region used for measuring the current transients

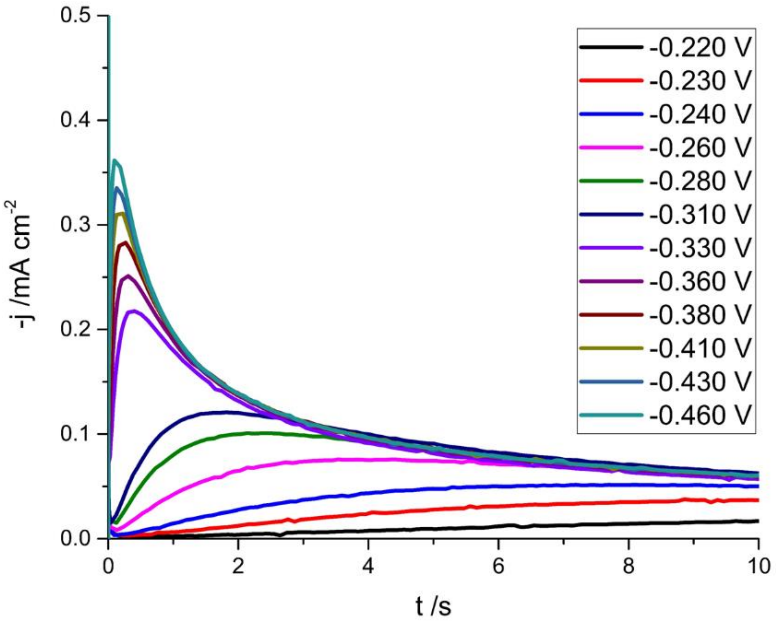

Figure 2. Current transients of tin electrodeposition on a boron doped diamond surface in 0.1 M H_2SO_4 and 0.5 mM $SnSO_4$. Transients were recorded between -0.220 to -0.460 V. For each transient, the respective potential was applied during 1 min, and it was followed by applying 0.14 V during 3 minutes to dissolve the deposit. Dissolution of the tin deposit was carried out before applying each respective potential.

The current transients are analyzed by comparison to the well-established Scharifker-Hills (SH) model[12]. The SH model considers nuclei of hemispherical shape, whose growth is controlled by three-dimensional diffusion. Two limiting cases of nucleation and growth are described by the model: instantaneous and progressive.

The nucleation rate is described by:

$$N(t) = N_o(1 - e^{-At}) \quad (1)$$

where *N* is the number of nuclei, N_0 the number of nucleation sites, and *A* the nucleation rate constant. For instantaneous nucleation, all nuclei are formed at once when applying the step potential, so that $At >> 1$ and therefore $N(t) = N_o$. The current–time transient for instantaneous nucleation and growth is given by:

$$j(t) = \frac{zFD^{1/2}c}{\pi^{1/2}t^{1/2}}[1 - \exp(-N_o\pi\kappa Dt)] \quad (2)$$

where $\kappa = (8\pi cM/\rho)^{1/2}$, with c the concentration (of Sn^{2+}), M the molar mass, and ρ the molar density.

For progressive nucleation and growth, nuclei are gradually formed after applying the step potential, so that $At << 1$ and therefore $N(t) = AN_o t$. The current-time transient for progressive nucleation and growth is given by:

$$j(t) = \frac{zFD^{1/2}c}{\pi^{1/2}t^{1/2}}\left[1 - \exp\left(-\frac{2}{3}AN_o\pi\kappa Dt^2\right)\right] \quad (3)$$

By plotting current transients in normalized coordinates, $(\frac{j}{j_{max}})^2$ vs $\frac{t}{t_{max}}$, we avoid the use of the system-specific parameters (c, M, ρ, AN_0, N_0) in comparing the experimental transients with the two limiting cases[13]. The associated expressions for instantaneous and progressive nucleation are described by equations (4) and (5)[13], [14] respectively:

$$\frac{j^2}{j^2{}_{max}} = 1.9542\,(\frac{t}{t_{max}})^{-1}\left[1 - \exp\,(-1.2564\frac{t}{t_{max}})\right]^2 \quad (4)$$

with $j_{max} = 0.6382zFDc(kN)^{1/2}$ and $t_{max} = 1.2564/N\pi kD$ for instantaneous nucleation

$$\frac{j^2}{j^2{}_{max}} = 1.2254\,(\frac{t}{t_{max}})^{-1}\left[1 - \exp\,(-2.3367\frac{t^2}{t^2{}_{max}})\right]^2 \quad (5)$$

with $j_{max} = 0.4959zFD^{3/4}c(kaN_0)^{1/4}$ and $t_{max} = (3.505/aN_0\pi kD)^{1/2}$ for progressive nucleation.

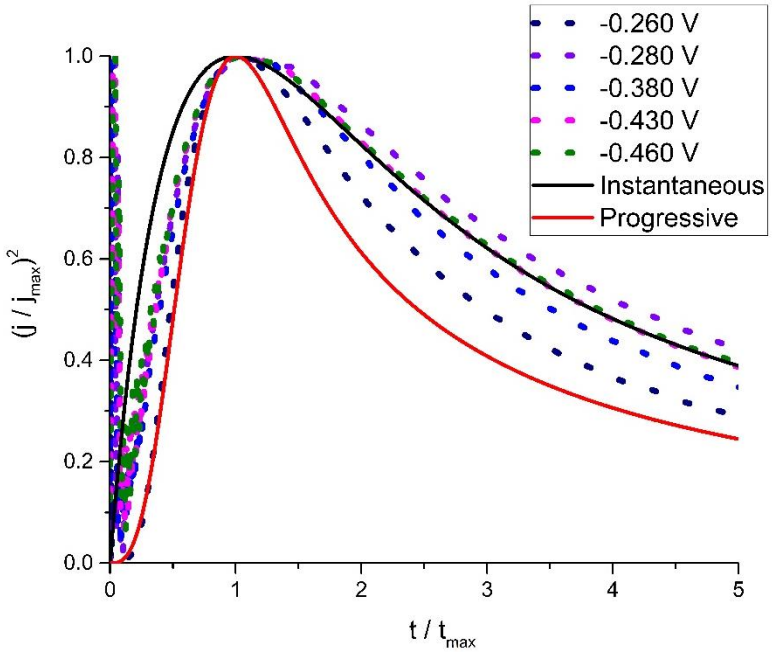

Figure 3. Normalized current transients calculated with SH model for the limiting cases (solid lines) compared with the normalized experimental transients (dotted lines). Experimental transients were recorded in 0.1 M H_2SO_4 and 0.5 mM $SnSO_4$.

Figure 3 shows the comparison of normalized current transients for tin deposition on boron doped diamond from low to high overpotentials compared to the instantaneous and progressive nucleation limiting cases. For a potential of -0.260 V, it is seen that at short times the experimental transient curve satisfactorily overlaps with the progressive nucleation mechanism. However, at longer times the experimental curve deviates from the progressive nucleation mechanism. Furthermore, at higher overpotentials and shorter times, the experimental current transients do not satisfactorily fit with neither the progressive nor the instantaneous nucleation mechanisms. But at longer times, the experimental curves fit better with the instantaneous mechanism. Figure 3 also shows the transition from progressive to instantaneous nucleation with increasingly negative potential. This behavior is also indicative that the electrode surface (and the number of nucleation sites) is not changing considerably with potential. In order to confirm the transition from progressive to instantaneous nucleation when increasing the negative potential, the first and second derivatives of the current transients at less and more negative potentials were calculated. For a progressive nucleation and growth mechanism, one expects a positive second derivative at short times, whereas for instantaneous nucleation, the second derivative should be negative at short times. Figure 4 shows the second derivative (blue dotted line) for the onset of the transient (short times) for various potentials, showing that the transition to instantaneous nucleation and growth happens at a potential of ca. -0.33 V. Figures 4c and 4d exhibit high noise level at short times (i.e. < 0.2 s) as a consequence of the charge-discharge double layer process. The noise level also increases during the derivation process.

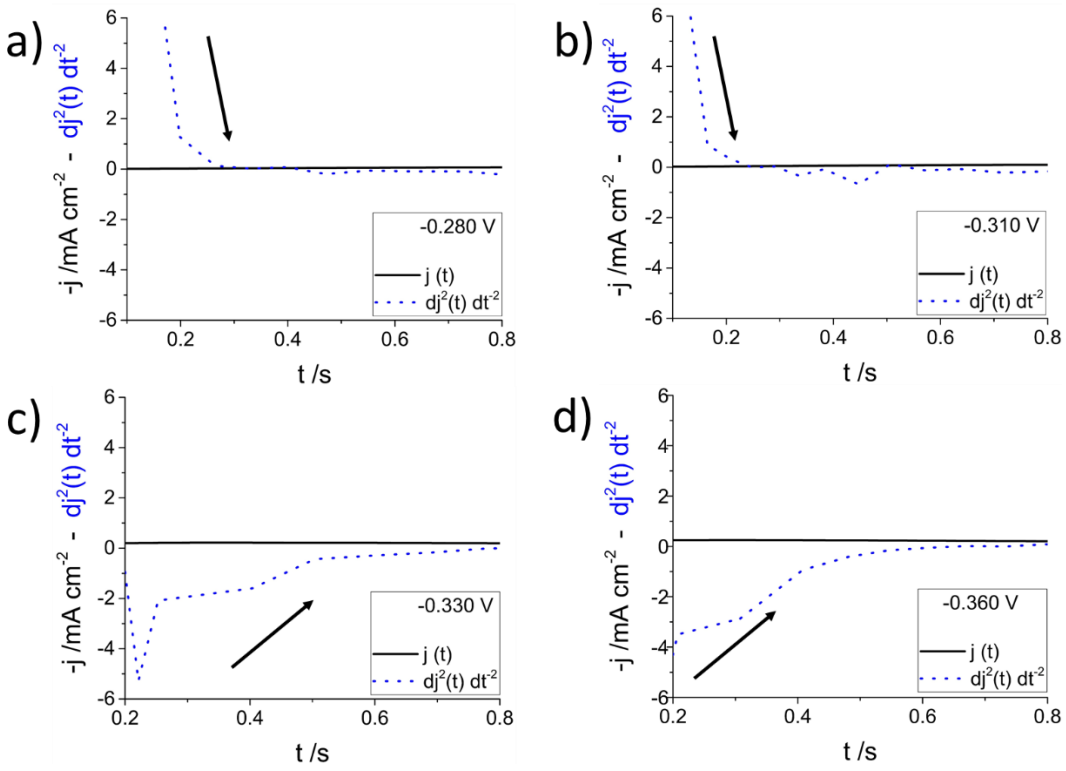

Figure 4. Current transient j(t) and second derivative $\frac{d^2 j(t)}{dt^2}$ for current transients recorded in 0.1 M H_2SO_4 and 0.5 mM $SnSO_4$ at (a) -0.280 V (b) -0.310 V (c) -0.330 V and (d) -0.360 V

Although the SH model equations do not perfectly fit the recorded current transients, a reasonable fitting is reached at high overpotentials and long times. The recorded transients were fitted by hand to the expressions for instantaneous and progressive nucleation and growth, equations 2 and 3, respectively. Current transients recorded at potentials > -0.3 V were fitted to the progressive nucleation, and at potentials < -0.3 V to the instantaneous. No attempt was made to perform a least-squares fit because the fit is never perfect, as can be seen from Figure 3. Instead, the steady state nucleation rate[15] (AN_0) and the number density of nuclei (N_0) were estimated from the corresponding expressions of t_{max} , see equations 4 and 5 .

Figure 5 presents the SH model curves for progressive nucleation and growth fitted to the measured current transients. At -0.230 V (low negative potential) and short times the theoretically predicted curve adequately fits the recorded transient, but at longer times the overlap is less good. Furthermore, with increasing the negative potentials, it is seen that the theoretically predicted transients adjust better to the experimental transients, from -0.360 V to higher overpotentials, curves tend to merge at higher times (i.e., >1s)

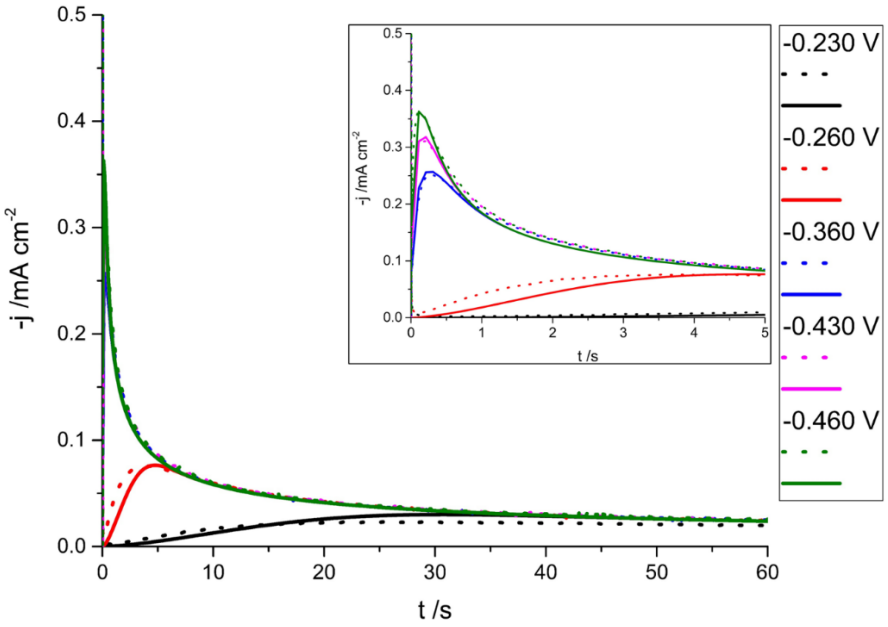

Figure 5. SH expression for progressive nucleation and growth (solid lines) fitted to recorded current transients (dotted lines) for tin electrodeposition on a boron doped diamond surface in 0.1 M H_2SO_4 and 0.5 mM $SnSO_4$. Given that there is never a very good excellent fit (Fig.3), these fits were performed "by hand", transients recorded at E > -0.3 V were fitted to progressive and at E < -0.3 V to instantaneous nucleation mode. The parameters N_0 and AN_0 shown in Figure 6 were, however, not obtained from the fit, but from the corresponding expressions for t_{max} (see main text).

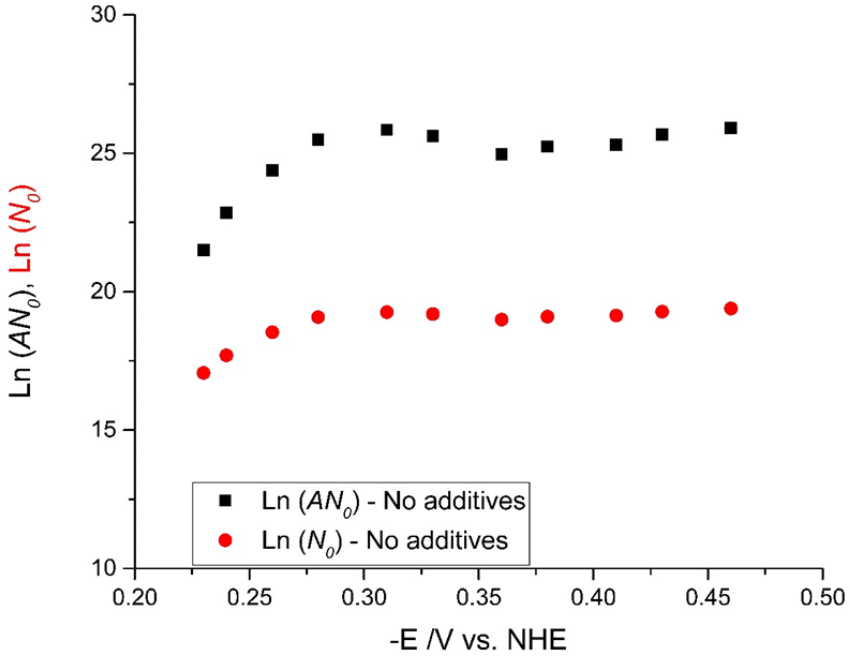

Figure 6. Logarithm of steady state nucleation rate (AN_o) versus applied potential and the Logarithm of number density of nuclei (N_0) versus applied potential of tin electrodeposition on a boron doped diamond surface in 0.1 M H_2SO_4 and 0.5 mM $SnSO_4$

Figure 6 shows the logarithm of the steady state nucleation rate (AN_0) and number density of nuclei (N_0) plotted versus the applied potential. The parameters AN_0 and N_0 were obtained from the corresponding expressions for t_{max} (see equations 4 and 5). It is observed that both AN_0 and N_0 exhibit an approximately linear increase at potentials below -0.28 V, and remain essentially constant at potentials more negative than -0.30 V. This transition potential corresponds reasonably well to the transition from progressive to instantaneous nucleation evaluated in Figure 4c. Therefore, we consider the AN_0 data more meaningful for potentials > -0.3 V and the N_0 data for potentials < -0.3 V. The atomistic theory of nucleation predicts a linear dependence of the logarithm of the steady state nucleation rate (AN_0) on the overpotential at high supersaturation[16]. Figure 6 indeed exhibits a linear dependence of the steady state nucleation rate on the applied potential in the window where the AN_0 data are meaningful. The data for E < -0.3 V, where the data for N_0 is more meaningful, show that N_0 is essentially constant over a wide potential window.

An alternative way to determine these parameters is to fit the initial part of the transient to a general nucleation equation. Sluyters-Rehbach et al.[17] described a general equation of nucleation and diffusion-controlled hemispherical growth, and employed a graphical analysis of the current transients: ($j^{2/3}$ vs t) and (j^2 vs t) to check the consistency between the model and the experimental transients and also to determine whether one of the two nucleation limiting cases, vis. instantaneous or progressive, predominates. This offers a more accurate way of determining parameters such as A and N_0. However, given the high double-layer current at short times, the values of the parameters A and N_0 were difficult to extract, and since we were primarily interested in the qualitative behavior of A and N_0, deriving them from t_{max} served our purposes well.

4.3.2 Effect of naphthalene-based additives on kinetics of tin electrodeposition on BDD

In order to study the effect of naphthalene-based additives on the kinetics of tin electrodeposition on a boron doped diamond electrode, current transients of tin electrodeposition were recorded in the presence of three different additives: NPT, NPTS and HNPTS. Figure 7a, 7b and 7c show current transients recorded at highly negative potential (-0.460 V) in the presence of different concentrations of NPT, NPTS and HNPTS, respectively, and Figure 7d shows the comparison of the different naphthalene-based additives.

Figure 7a shows transients in the absence and presence of NPT at different concentrations. Transients exhibit an increase of t_{max} and decrease of i_{max}, ascribed to a decrease in the nucleation rate of tin deposition on BDD. The transients do not show a remarkable dependence on the NPT concentration which we attribute to the low solubility of NPT molecules in the aqueous electrolyte, leading to the same bulk concentration and thereby limiting the amount of NPT available that can be adsorbed on BDD surface. Furthermore,

current transients in the absence and in the presence of different NPT concentrations overlap after about 1.5 seconds.

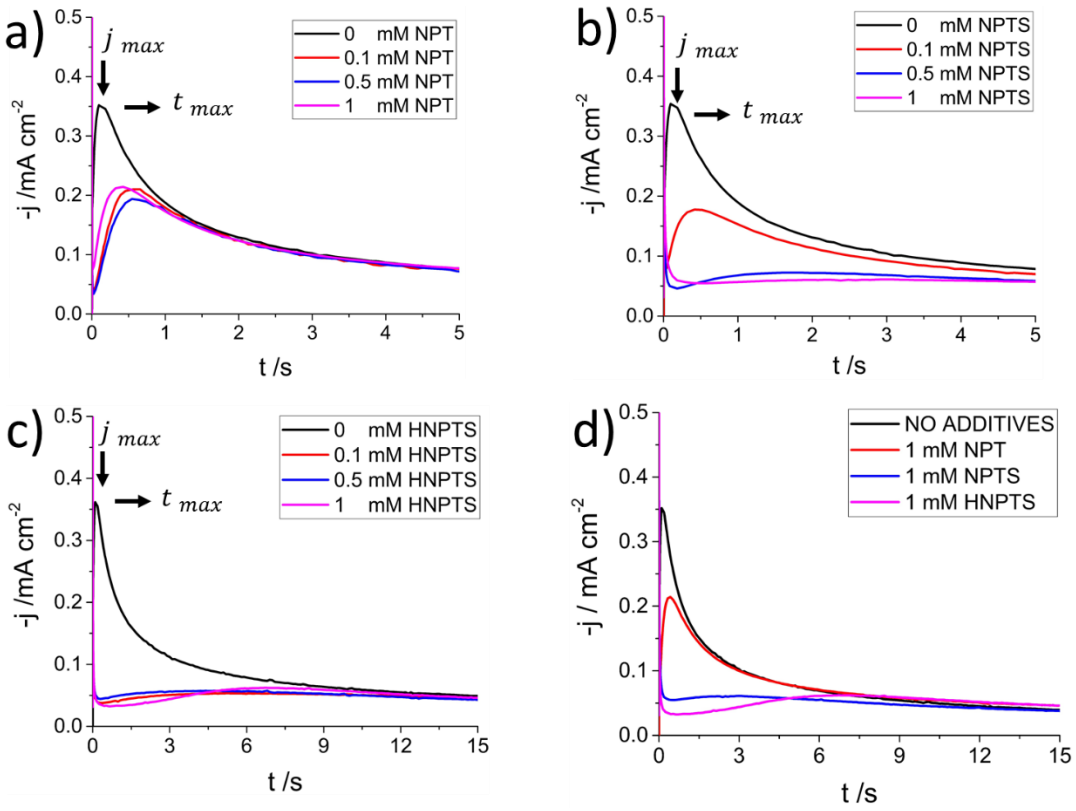

Figure 7. Current transients recorded at highly negative potential (-0.460 V) of tin electrodeposition on a boron doped diamond surface in 0.1 M H_2SO_4, 0.5 mM $SnSO_4$ and different naphthalene-based concentrations: (a) NPT, (b) NPTS and (c) HNPTS (d) Comparison of transients in the absence and presence of 1 mM naphthalene-based additives

Figure 7b shows transients in the absence and presence of NPTS. Parameters t_{max} and i_{max} increase and decrease, respectively, with increasing NPTS concentration. This change is also ascribed to a decrease in the nucleation kinetics of tin deposition. The transient in the presence of 1 mM of NPTS looks almost flat in comparison to the other transients. Figure 7c presents the transients in the absence and presence of HNPTS; transients exhibit a much stronger decrease in i_{max} and increase in t_{max} compared to the transients in the presence of NPT and NPTS. Additionally, Fig. 7d compares the different additives in a single figure, clearly illustrating the evolution of the transient as a function of the additive.

For long deposition times, the SH model assumes the growth of the deposit to be completely diffusion limited. Therefore, tin (II) diffusion coefficients ($D_{Sn^{2+}}$) can be calculated in the presence of different concentrations of naphthalene-based additives by fitting the transient to the Cottrell equation. The results are summarized in Table C1 in the Appendix C.

The equation was applied for the transients at -0.460 V, and at times longer than 15 s to avoid contributions from nucleation kinetics. A plot of j vs. $t^{-1/2}$ yields a straight line in all cases. The calculated value of tin (II) diffusion coefficient ($D_{Sn^{2+}}$) in the absence of naphthalene-based additives is 7.7 ± 0.2 X 10^{-6} cm^2 s^{-1}, which is in accordance with previously determined values[3] [1], and the values in the presence of 1mM of NPT, NPTS and HNPTS are 6.8 X 10^{-6}, 7.0 X 10^{-6} and 7.3 X 10^{-6} cm^2 s^{-1} respectively, all in reasonable agreement. In the presence of different concentrations of HNPTS, the calculated tin (II) diffusion coefficient ($D_{Sn^{2+}}$) also does not change considerably. Furthermore, when tin (II) diffusion coefficients ($D_{Sn^{2+}}$) are calculated from transients obtained at less negative potentials in the presence of the naphthalene-based additives, no significant differences were observed, see Table C2. These results suggest that naphthalene-based additives do not affect the diffusion coefficient nor the kinetics of tin deposition on BDD electrode; they only affect the nucleation rate.

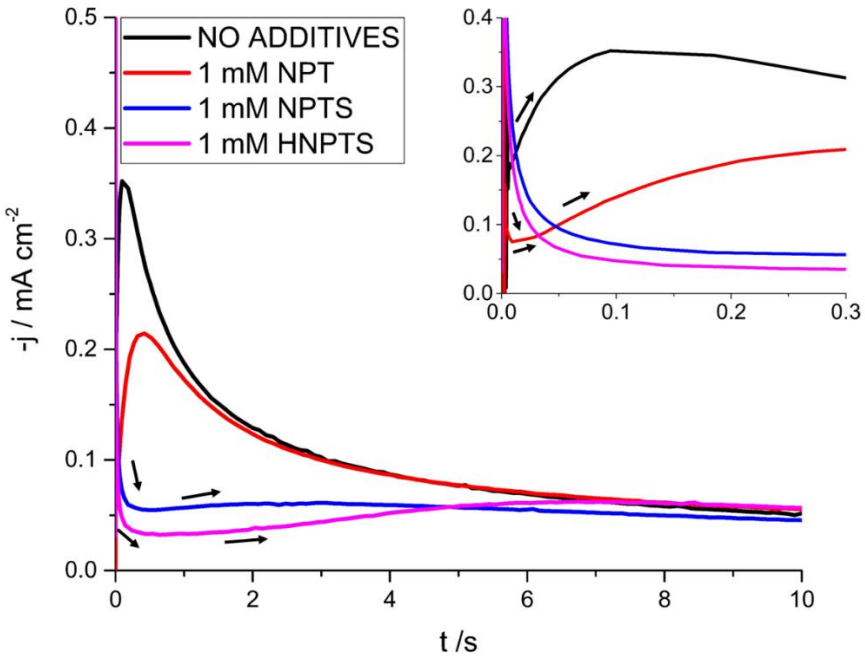

Figure 8. Onset of the current transients recorded in 0.1 M H_2SO_4, 0.5 mM $SnSO_4$ at high negative potentials E=-0.460 V, in the absence and presence of 1 mM of NPT, NPTS, and HNPTS at -0.460 V.

Figure 8 shows the onset of the current transients recorded in the absence and presence of naphthalene-based additives. The onset of the current transients in the presence of NPTS and HNPTS clearly show the progressive nucleation behavior, where current gradually increases when new nuclei originate. The black arrows indicate the increasing growth of the current typical for progressive nucleation. On the other hand, the onset of the transient in the presence of NPT (Inset of Fig. 8) is more characteristic of instantaneous nucleation. See analysis of the second derivative for NPT, NPTS and HNPTS in the Figure S1.

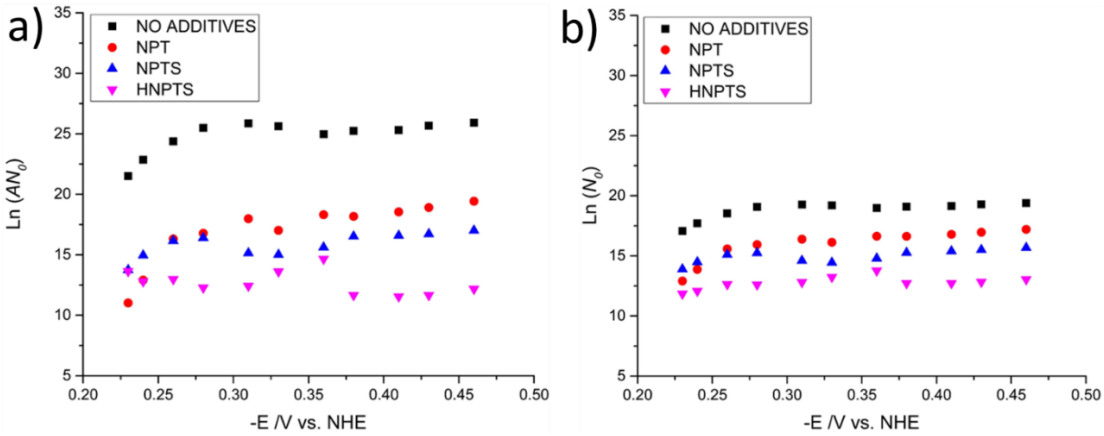

Figure 9. Dependence of logarithm of (a) steady state nucleation rate (AN_0) and (b) number density of nuclei (N_0) on the applied potential for tin electrodeposition on a boron doped diamond surface in 0.1 M H_2SO_4 and 0.5 mM $SnSO_4$ in the absence and presence of 1 mM of: NPT, NPTS and HNPTS. The steady state nucleation rate (AN_o) and the number density of nuclei (N_0) were obtained from times of the maximum of the current transients by using Eqs. 4 and 5.

Figure 9 shows the relationship between the logarithm of (AN_o) and (N_0) and the applied potential in the presence of the different naphthalene-based additives NPT, NPTS and HNPTS, as determined from the expressions for t_{max}, Eqs. 4 and 5. As expected, a considerable decrease of the steady state nucleation rate (AN_0) or the number density of nuclei (N_0) is observed in the order NPT > NPTS > HNPTS.

Although the fit with the SH nucleation and growth expressions is never perfect, the analysis above shows that the naphthalene-based additives act primarily on the nucleation probability, and that the diffusion limited growth of formed nuclei is not affected by the additive.

4.3.3 Scanning electron microscopy

Scanning electron micrographs were recorded to image the morphology of the tin deposits on BDD in the absence and presence of naphthalene-based additives.

Figure 10a and 10b shows the BDD surface before the tin deposition. Surface defects such as cracks, holes and grain boundaries are visible. Large flat areas of about ~ 1 X 1 µm are also seen. The BDD surface in general exhibits lighter and darker zones which correlated with zones of lower and higher conductivity[7]. By scanning large enough areas, both types of surfaces can be observed in a single image[7]. Images reported here are representative of several images taken over the BBD electrode surface.

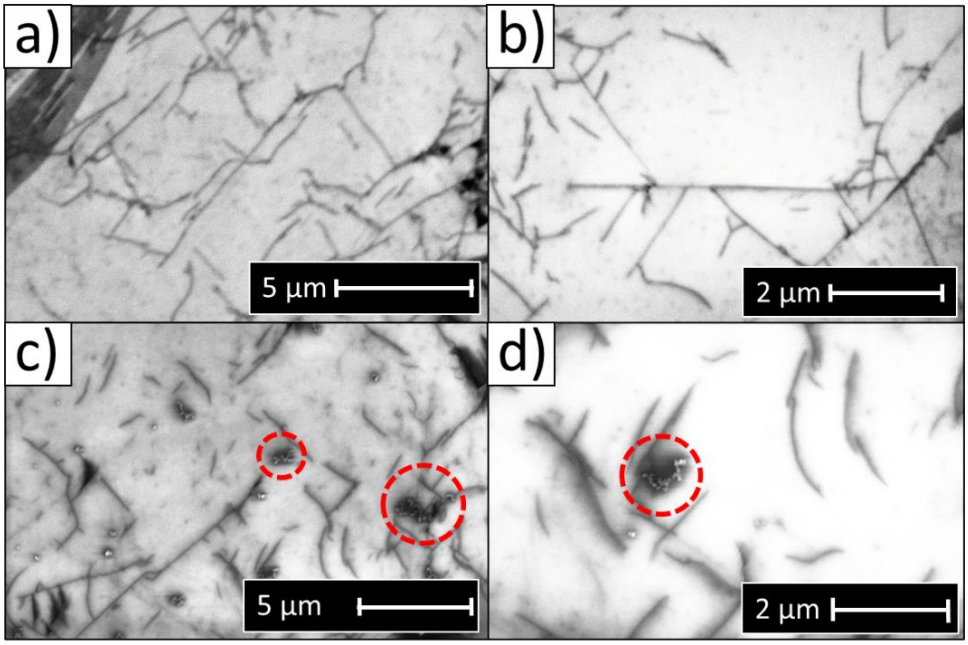

Figure 10. Scanning electron micrographs of BDD surface before tin deposition (a, b) and after tin deposition (c, d). Deposition was performed in 0.1 M H_2SO_4 and 0.5 mM $SnSO_4$. Potential was held at -0.266 V for 10 s where nucleation and early growth happened, subsequently the potential was held at -0.230 V during 60 s where the nuclei were grown.

Figure 10c and 10d show tin crystallites on BDD surface, obtained in the absence of surfactants by holding the potential at -0.266 V for 10 s at which nucleation and early growth happened, after which the potential was stepped back to -0.230 V during 60 s, at which potential the nuclei were grown further. Figs. 10c and d show how crystallites cluster together at or near the darker defect areas of higher conductivity. The size of the crystallites is approximately ~50 nm diameter and does not change substantially over the electrode surface.

Figure 11a presents the tin deposits on BDD in the absence of naphthalene-based additives. Unlike tin deposits grown in the absence of additives, tin electrodeposited in the presence of NPT on BDD (Fig. 11b) exhibits crystallites over the entire surface, not only near the surface defects but also on the large flat areas. Nonetheless, tin deposition is still preferred around the defects, where clusters of crystallites are seen mainly on the cracks and holes. Furthermore, a larger distribution of crystallite shapes is noticeable. Figure 11c shows the tin deposit grown in the presence of NPTS, tin crystallites are visible near the surface defects and on the large flat areas; crystallites seem to have a specific shape and exhibit a higher distribution and bigger sizes (~100 nm) than in the absence and presence of NPT.

Tin deposits grown in the presence of HNPTS are shown in Figure 11d. Tin crystallites grow mainly near the defects; crystallites exhibit a larger size distribution (~100 to ~500 nm) which indicates that they were not formed at the same time, i.e., the progressive nucleation mode is operative.

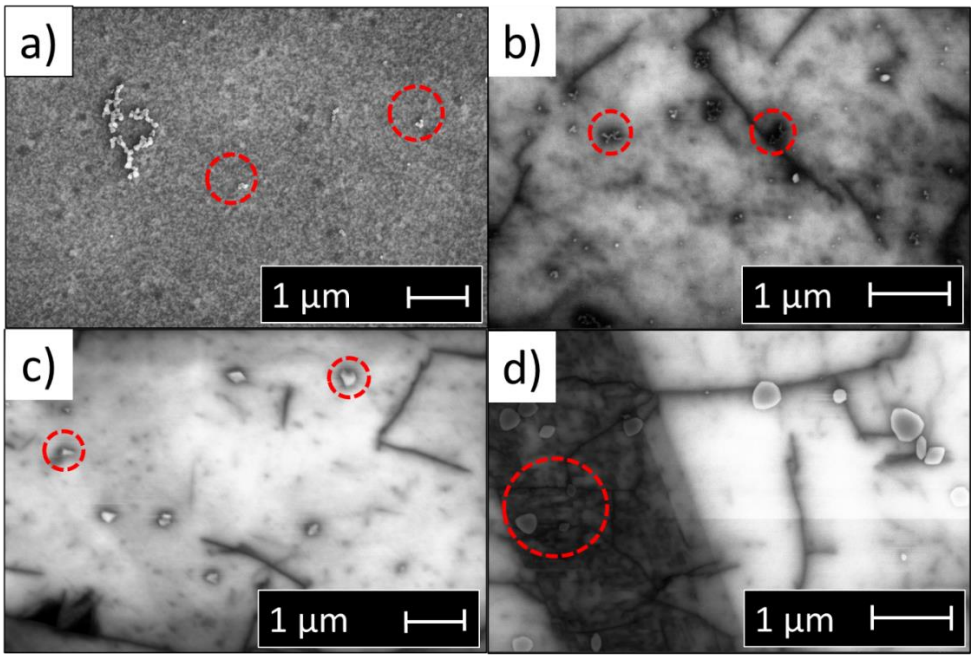

Figure 11. Scanning electron micrographs of tin electrodeposited on a boron doped diamond surface in 0.1 M H_2SO_4 and 0.5 mM $SnSO_4$: (a) in the absence of naphthalene-based additives (b) in the presence of 1 mM of NPT, (c) 1 mM NPTS, (d) 1 mM HNPTS. Potential was held at -0.266 V for 10 s where nucleation and early growth happened, subsequently the potential was held at -0.230 V during 60 s where the nuclei were grown.

Finally, the effect of ethoxylated α-napthalenesulfonic acid (ENSA), a commonly used additive in the tin electroplating industry, was also studied during tin electrodeposition on a boron doped diamond electrode. Figure 12a shows the current transient of tin electrodeposition recorded in the presence of ENSA; an almost complete inhibition of the tin deposition is seen (note that the currents are much lower than in Fig.7). Transients are essentially flat, the absence of t_{max} and i_{max} does not allow to compare these results to the standard nucleation and growth model of SH. Furthermore, the SEM image in Figure 12b confirms the inhibition of the tin electrodeposition on Boron doped diamond electrode in the presence of ENSA. Hardly any tin crystallites (in fact only one) are seen in the micrograph.

4.3.4 Comparison to tin electrodeposition on gold

The above results are in partial agreement with our previous work on the effect of naphthalene-based additives on tin electrodeposition on gold[6]. In our previous study, we showed that on gold surfaces, NPT and NPTS lie flat on the surface and interact mainly via van der Waals forces, with NPTS molecules, forming a more compact structure due to intermolecular lateral interactions. Thus, one can expect that on BDD, NPT and NPTS might

also lie flat, since van der Waals interactions are not very sensitive to the electrode surface. Also, the intermolecular lateral interactions between NPTS molecules are not expected to change significantly on BDD. The results on BDD show that a more compact film formed in the presence of NPTS decreases the nucleation kinetics more than NPT.

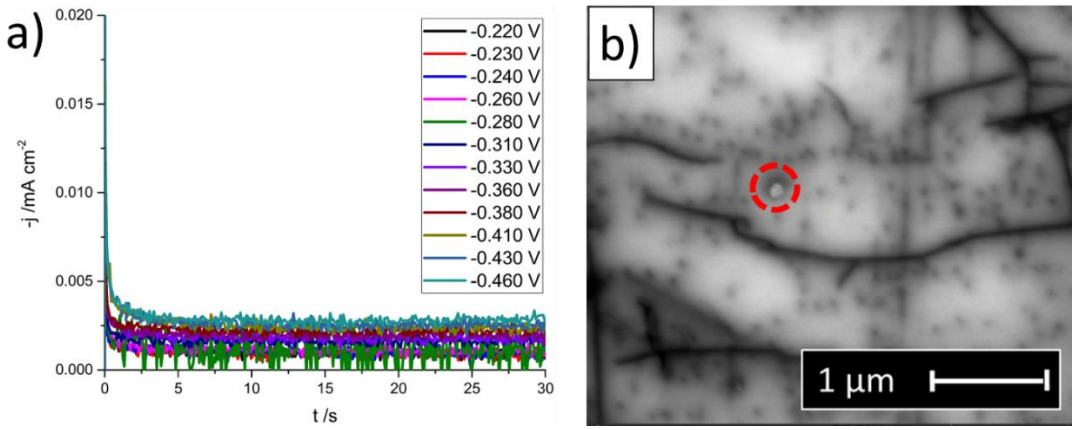

Figure 12. (a) Current transients of tin electrodeposition on a boron doped diamond surface in the presence of 1 mM ENSA, 0.1 M H_2SO_4, 0.5 mM $SnSO_4$, recorded between -0.220 to -0.460 V. (b) Scanning electron micrograph of tin electrodeposited on a boron doped diamond surface in 0.1 M H_2SO_4 and 0.5 mM $SnSO_4$ and in the presence 1 mM of ENSA. The potential was held at -0.266 V for 10 s, subsequently the potential was held at -0.230 V during 60 s.

With respect to HNPTS, our work on gold showed[6] it does not lie flat on the surface, but rather that the naphthol group undergoes reductive desulfonation and subsequent polymerization via crosslinked reactions. Since polymerization processes are not highly sensitive to the electrode surface, a polymeric film is likely to form in the presence of HNPTS on BDD. Furthermore, ethoxylated α-napthalenesulfonic acid (ENSA) shows equivalent polymer film formation, and indeed tin electrodeposition on BDD is highly inhibited in its presence.

The effect of naphthalene-based additives on the kinetics of tin electrodeposition on boron doped diamond is complementary to our previous work on gold electrodes[6], giving insights on the way naphthalene-based additives affect the kinetics of tin electrodeposition process. On gold, the nucleation process appeared to be too fast to obtain meaningful transients. In this study, we were able to show that NPT, NPTS and HNPTS mainly have an effect on the nucleation process. Moreover, although the transients in the presence of ethoxylated α-napthalenesulfonic acid (ENSA) could not be compared to the standard nucleation and growth model of Scharifker and Hills, ENSA exhibits a very similar behavior to that on gold, i.e., a strong inhibition of the tin electrodeposition process.

4.4 Conclusions

The effect of naphthalene (NPT), naphthalenesulfonate (NPTS) and hydroxynaphthalenesulfonate (HNPTS) on the kinetics of tin electrodeposition on a boron doped diamond electrode has been studied by using chronoamperometry and scanning electron microscopy (SEM). The potentiostatic current transients were analyzed with the standard Scharifker-Hills model, giving the steady state nucleation rate (AN_0) and the number density of nucleation sites (N_0) at different applied potentials. In the absence of additives, the nucleation and growth process is shown to transition from progressive to instantaneous with increasingly negative potential. A decrease in the nucleation kinetics of tin deposition on BDD was observed in the presence of naphthalene-based additives: NPT showed the smallest effect on the reduction of the kinetics, followed by NPTS, and the strongest effect was observed in the presence of HNPTS. Analysis with the Scharifker-Hills model, shows that the steady-state nucleation rate and the number density of nucleation sites exhibit the expected decrease in the presence of the different naphthalene-based additives over the entire studied potential range. Additionally, tin (II) diffusion coefficients were determined by fitting the current transients at longer times to the Cottrell equation, the calculated values of tin (II) diffusion coefficient ($\mathrm{D}_{\mathrm{Sn}^{2+}}$) giving similar values in the absence and presence of the additives. This observation indicates that tin (II) is not complexed by the additives. Moreover, similar values of tin (II) diffusion coefficients were obtained at low negative potentials, suggesting that also the charge-transfer kinetics itself is not influenced by the presence of the additives. The additives only affect the nucleation process. Ethoxylated α-napthalenesulfonic acid (ENSA) strongly inhibits the tin electrodeposition process, similar to deposition on gold, yielding transients that cannot be analyzed with the Scharifker-Hills model.

4.5 References

(1) Walsh, F. C.; Low, C. T. J. A Review of Developments in the Electrodeposition of Tin. *Surf. Coatings Technol.* **2016**, *288*, 79–94.

(2) Tzeng, G. S.; Lin, S. H.; Wang, Y. Y.; Wan, C. C. Effects of Additives on the Electrodeposition of Tin from an Acidic Sn(II) Bath. *J. Appl. Electrochem.* **1996**, *26* (4), 419–423.

(3) Barry, F. J.; Cunnane, V. J. Synergistic Effects of Organic Additives on the Discharge, Nucleation and Growth Mechanisms of Tin at Polycrystalline Copper Electrodes. *J. Electroanal. Chem.* **2002**, *537* (1–2), 151–163.

(4) Wen, S.; Szpunar, J. A. Nucleation and Growth of Tin on Low Carbon Steel. *Electrochim. Acta* **2005**, *50* (12), 2393–2399.

(5) Wijenberg, J. H. O. J. Initial Stages of Electrochemical Phase Formation, Utrech, 1991.

(6) Aranzales, D.; Briliani, I.; McCrum, I. T.; Wijenberg, J. H. O. J.; de Vooys, A. C. A.; Koper, M. T. M. The Effect of Naphthalene-Based Additives on Tin Electrodeposition on a Gold Electrode. *Electrochim. Acta* **2021**, *368*, 137606.

(7) Hyde, M. E.; Jacobs, R.; Compton, R. G. In Situ AFM Studies of Metal Deposition. *J. Phys. Chem. B* **2002**, *106* (43), 11075–11080.

(8) Enea, O.; Riedo, B.; Dietler, G. AFM Study of Pt Clusters Electrochemically Deposited onto Boron-Doped Diamond Films. *Nano Lett.* **2002**, *2* (3), 241–244.

(9) Simm, A. O.; Ji, X.; Banks, C. E.; Hyde, M. E.; Compton, R. G. AFM Studies of Metal Deposition: Instantaneous Nucleation and the Growth of Cobalt Nanoparticles on Boron-Doped Diamond Electrodes. *ChemPhysChem* **2006**, *7* (3), 704–709.

(10) Zak, J.; Kolodziej-Sadlok, M. AFM Imaging of Copper Stripping/Deposition Processes in Selected Electrolytes on Boron-Doped Diamond Thin-Film Electrodes. *Electrochim. Acta* **2000**, *45* (17), 2803–2813.

(11) Milchev, A. *ELECTROCRYSTALLIZATION Fundamentals of Nucleation and Growth*; Kluwer Academic Publishers: New York, Boston, Dordrecht, London, Moscow, 2002.

(12) Scharifker, B. R.; Mostany, J. Three-Dimensional Nucleation with Diffusion Controlled Growth: Part I Three-Dimensional Nucleation and Nucleation Rates per Site. *J. Electroanal. Chem.* **1984**, *177*, 13–23.

(13) Scharifker, B. Theoretical and Experimental Studies of Multiple Nucleation. *Electrochim. Acta* **1982**, *28* (2), 879–889.

(14) Scherb, G.; Kolb, D. M. Cu Deposition onto N-GaAs(100): Optical and Current Transient Studies. *J. Electroanal. Chem.* **1995**, *396* (1–2), 151–159.

(15) Milchev, A. Electrochemical Nucleation on Active Sites - What Do We Measure in Reality? Part I. *J. Electroanal. Chem.* **1998**, *457* (1–2), 35–46.

(16) Milchev, A.; Stoyanov, S.; Kaischev, R. Atomistic Theory of Electrolytic Nucleation: I. *Thin Solid Films* **1974**, *22* (3), 255–265.

(17) Sluyters-Rehbach, M.; Wijenberg, J. H. O. J.; Bosco, E.; Sluyters, J. H. The Theory of Chronoamperometry for the Investigation of Electrocrystallization. Mathematical Description and Analysis in the Case of Diffusion-Controlled Growth. *J. Electroanal. Chem.* **1987**, *236* (1–2), 1–20.